

Momentum dependence of the Stoner excitation spectrum of iron using spin-polarized electron-energy-loss spectroscopy

D. Venus* and J. Kirschner

Institut für Grenzflächenforschung und Vakuumphysik, Kernforschungsanlage Jülich, D-5170 Jülich, Federal Republic of Germany

(Received 23 July 1987)

The electron-hole excitations with different spin configurations have been separated and studied experimentally in iron, with use of spin-resolved electron-energy-loss spectroscopy with both a source and detector of spin-polarized electrons. The data are interpreted using a two-particle, exchange scattering model, and analyzed in the 4×4 product spin space of the incident and target electrons. Stoner excitations in the form of majority-hole–minority-electron pairs are found to comprise up to one-third of the total electron-hole excitations in off-specular scattering, and exhibit a clear, broad peak due to excitations within the exchange-split d bands of iron. The width and energy loss at which this peak occurs increase with increasing wave vector of the Stoner excitation. These trends are also observed in the calculated Stoner density of states for iron.

I. INTRODUCTION

Two of the most important characteristics of itinerant-electron magnetism are the dramatic effects of electron-electron interactions, and the ability of the magnet to support magnetic excitations. The first of these properties leads to separate electronic bands for the spin-up and spin-down electrons. These may be described as perturbations of a degenerate, paramagnetic band structure from which the energy degeneracy is lifted by an “exchange splitting” which is dependent on spin and wave vector. When the Fermi level lies between the bands derived from a single degenerate paramagnetic band, the lower energy, spin-up (or majority) states are occupied, while the higher energy, spin-down (minority) states are not. This leads to a net spin polarization of the conduction electrons which supports the macroscopic magnetization.¹ Bands which are exchange split across the Fermi level also lead to the possibility of a unique single-particle excitation. An electron may be removed from an occupied majority state, undergo spin reversal, and be placed in a previously unoccupied minority state. The resulting electron-hole pair with opposed spin and net wave vector \mathbf{q} is termed a “Stoner excitation.” For each \mathbf{q} and spin combination, a distribution of Stoner excitations is possible. This distribution is called the “Stoner density of states,”¹ and is given by the joint density of states for occupied and unoccupied states of appropriate spin, with the momentum transfer \mathbf{q} . The most straightforward case is $\mathbf{q}=\mathbf{0}$, where the Stoner density of states shows the abundance distribution of the exchange splitting averaged over the Brillouin zone.

A second attribute of Stoner excitations is that, since they involve a spin reversal, they are the fundamental single-particle magnetic excitations in itinerant-electron magnetism. At low energy and wave vector, the configuration of the electronic bands does not allow individual Stoner excitations. In this case, the coherent superposition of virtual Stoner excitations of wave vector \mathbf{q}

can produce a collective magnetic excitation of wave vector \mathbf{q} (or spin wave) at low energy.³ The spin waves may be observed by means of inelastic neutron scattering.⁴ In regions of energy-momentum space where individual Stoner excitations are allowed, the spin wave and Stoner modes are coupled, so that the former are heavily damped.^{1,2,5}

Given that Stoner excitations play such a fundamental role in understanding both the ground state and magnetic excitations of itinerant-electron magnets, it is clear that an experimental probe of their excitation spectrum is desirable. Except in special cases,⁶ the range of energy and momentum occupied by these one-particle excitations makes it very difficult to study them by neutron scattering. Inelastic electron scattering has long been proposed as an alternate technique for studying magnetic excitations,⁷ but, until recently, most work has concentrated on the investigation of spin waves. It was thought that scattering from the magnetization density via the exchange potential⁸ would provide sufficient coupling between the incident electrons and the spin waves to allow the detection of the spin waves. Despite concerted effort,⁹ and the development of very-high-resolution electron-energy-loss spectroscopy (EELS) spectrometers, spin waves have never been observed by inelastic electron scattering.

In 1982, Yin and Tosatti¹⁰ focused attention, instead, on the study of Stoner excitations using EELS. In their model, an electron in the probe beam may scatter inelastically via the Coulomb interaction with a “target” electron of opposite spin bound in an occupied state of the crystal. If the incident electron loses a large fraction of its energy, it will fall into an unoccupied state just above the Fermi level and transfer this energy to the electron of opposite spin. The target electron may now have enough energy to escape from the solid and be detected. After this two-particle exchange scattering event, the crystal is in an excited state which corresponds to a Stoner electron-hole pair of momentum \mathbf{q} . It is important to note, however, that although the inter-

change of the incident and target electron gives the appearance of a spin flip, no electron has undergone a true reversal of spin. A compilation of these events as a function of the energy loss and momentum change of the scattered electron yields the Stoner density of states weighted by the electron-scattering matrix element.

Since the signature for the Stoner excitations is that the incident and scattered electrons have opposite spin, it is necessary to use a spin-polarized incident beam, and to detect the spin polarization of the scattered beam in order to isolate the Stoner excitations from the other possible inelastic scattering processes. The first experiments investigating Stoner excitations by EELS used either a spin-polarized electron source,¹¹ or a spin-polarization detector,¹² or neither,¹³ and argued that special conditions allowed the identification of the Stoner events in the model of Yin and Tosatti. Subsequent theoretical work by Mills¹⁴ stressed the importance of the surface in EELS, and suggested that some experimental results could be understood without recourse to spin-flip scattering. Vignale and Singwi¹⁵ concentrated on the excitation process in the bulk metal, and found qualitative agreement with the experiments. They emphasized that, for low-energy electrons, it should be possible to observe both Stoner excitations and spin waves for a range of q , even extending to $q=0$. Recent experiments by Kirschner¹⁶ and by Kirschner and Suga,¹⁷ who studied an iron crystal using both a source and a detector of spin-polarized electrons, finally provided an unambiguous identification of the spectrum of spin-flip events. They also demonstrated the feasibility of momentum-resolved, off-specular EELS experiments to determine the Stoner spectrum for finite wave vector. The results show that, for off-specular scattering, the Stoner events are almost as likely as scattering events not involving an apparent spin flip, and that their spectrum is a continuum which contains a broad peak centered at a loss energy of approximately 2 eV. This peak energy is in good agreement with other measurements of the exchange splitting in iron.¹⁸

The present paper gives a fuller account of the spin-polarized EELS experiments and presents new measurements obtained using a redesigned electron lens system which provides greater counting rates and a larger range of energy loss than in the original measurements. These improvements have resulted in a more complete data set and have made it possible to investigate the variation of the Stoner spectrum with the wave vector q . It is found that the spectrum for majority-hole-minority-electron Stoner excitations contains a clear, broad peak due to excitations within the exchange-split d bands. The width and energy loss at which this peak occurs are found to increase with increasing wave vector of excitation. These trends are also seen in the calculated Stoner density of states for iron. Measurement of this dispersion represents significant progress toward a mapping of the spectrum of single-particle magnetic excitations within the Stoner continuum. The remainder of the paper is divided into four sections. In Sec. II, a general description of spin-resolved, two-particle scattering is presented. This allows the separation of the Stoner exci-

tations from other inelastic scattering channels. In Sec. III the experimental apparatus, procedure, and data reduction are described. The Stoner spectra are analyzed in Sec. IV, and the work is summarized in Sec. V.

II. THEORY

In electron-energy-loss spectroscopy, a monoenergetic beam of electrons of energy E is directed onto a crystal surface and the scattered electrons are collected and counted as a function of energy and scattering angle.¹⁹ Most electrons are simply transmitted into the crystal and never reemerge. A few percent are reflected into the specular beam without loss of energy. A small fraction are reflected into the specular beam after having caused some elementary excitation of the solid. These electrons result in structure in the energy-resolved spectrum of the scattered electrons, and thus mark the energy of the excitation. This type of scattering occurs principally through the interaction of the electron with long-range, dipole electric fields which extend into the vacuum, and which are generated by surface atom or adsorbate vibrations, plasmons, or electron-hole pairs. This process has been very successfully described by a dielectric theory of surface dipole scattering.²⁰ Since the inelastic scattering actually occurs in the vacuum region, it is certain that the incident and scattered electron are one and the same. Because of this property, dipole scattering is a "direct" scattering mechanism.

An even smaller fraction of the incident electrons are scattered and emerge at an angle α to the specular direction after having caused some elementary excitation which involves both energy ϵ and crystal momentum q . If $\alpha > \epsilon/2E$, then the scattering occurs outside the main lobe of the dipole electric fields, and processes which are not described by the dielectric theory make a significant contribution to the total scattering. Electrons may enter the metal and undergo inelastic scattering through short-range interactions before elastic scattering from the ion cores redirects them into the vacuum once again. This type of short-range scattering is termed "impact" scattering. Since the emerging electron may or may not be the same one as was incident, impact scattering may be either a direct or an "exchange"-scattering mechanism.²¹ An approximate theory for direct scattering from phonons under these circumstances has been devised,²² but the excitation of electron-hole pairs is, as of yet, too complicated to treat quantitatively.

Leaving aside dipole scattering for the moment, the basic mechanism for the creation of electron-hole pairs in metals is electron-electron impact scattering via the screened Coulomb interaction. While the Coulomb interaction is independent of spin, the requirements of Fermi statistics and the presence of exchange-split bands in ferromagnets make the electron spin an important variable as well. If the incident electron has spin σ_i and unit amplitude as an incoming wave in the vacuum, and the target electron has spin σ_t , then the amplitude for the scattering event in which the incident electron creates an electron-hole pair and then escapes and is detected, may be denoted $f_{\sigma_i\sigma_t}(\eta, \epsilon, q)$.²² Here f indi-

cates that this is direct scattering, and η represents a set of quantum numbers which specify the initial and final states of both electrons. In general, $f_{\uparrow\uparrow}(\eta, \epsilon, \mathbf{q})$ and $f_{\uparrow\downarrow}(\eta, \epsilon, \mathbf{q})$ are not equal since, for exchange-split bands, a specified set of quantum numbers η will describe allowed eigenstates for only a spin-up target electron or a spin-down target electron. If, instead, the target electron escapes and is detected, then the scattering amplitude is denoted $g_{\sigma_i\sigma_f}(\eta, \epsilon, \mathbf{q})$, where g indicates exchange scattering. When $\sigma_i \neq \sigma_f$, the exchange events lead to a final state in which the electron and the hole remaining in the metal have opposite spin—a Stoner excitation. Since the direct and exchange scattering can be distinguished by the spin of the detected electron, the scattering amplitudes do not interfere quantum mechanically. When $\sigma_i = \sigma_f$, direct and exchange scattering lead to indistinguishable final states. The amplitudes for direct and exchange scattering therefore interfere.

The eight possible scattering amplitudes lead to four measurable scattering intensities, or scattering “channels.”¹⁰ Two of these are called “spin-flip” intensities since the scattered electron has undergone an exchange which appears to produce a spin flip. These are denoted by the letter F . Two channels are termed “spin-nonflip” intensities and are denoted by N :

$$F^{\downarrow}(\epsilon, \mathbf{q}) \text{—electron incident } \uparrow; \text{ electron detected } \downarrow, \quad (1a)$$

$$F^{\uparrow}(\epsilon, \mathbf{q}) \text{—electron incident } \downarrow; \text{ electron detected } \uparrow, \quad (1b)$$

$$N^{\uparrow}(\epsilon, \mathbf{q}) \text{—electron incident } \uparrow; \text{ electron detected } \uparrow, \quad (1c)$$

$$N^{\downarrow}(\epsilon, \mathbf{q}) \text{—electron incident } \downarrow; \text{ electron detected } \downarrow. \quad (1d)$$

When the experimental conditions are such that spin-orbit coupling in the metal does not affect the spin polarization of the diffracted beam, these partial intensities may be rewritten in terms of the two-particle scattering amplitudes. Assuming that multiple inelastic scattering may be neglected,

$$F^{\downarrow}(\epsilon, \mathbf{q}) = \sum_{\eta} |g_{\uparrow\downarrow}(\eta, \epsilon, \mathbf{q})|^2, \quad (2a)$$

$$F^{\uparrow}(\epsilon, \mathbf{q}) = \sum_{\eta} |g_{\downarrow\uparrow}(\eta, \epsilon, \mathbf{q})|^2, \quad (2b)$$

$$N^{\uparrow}(\epsilon, \mathbf{q}) = \sum_{\eta} |f_{\uparrow\uparrow}(\eta, \epsilon, \mathbf{q}) - g_{\uparrow\uparrow}(\eta, \epsilon, \mathbf{q})|^2 + |f_{\uparrow\downarrow}(\eta, \epsilon, \mathbf{q})|^2 \quad (2c)$$

$$N^{\downarrow}(\epsilon, \mathbf{q}) = \sum_{\eta} |f_{\downarrow\downarrow}(\eta, \epsilon, \mathbf{q}) - g_{\downarrow\downarrow}(\eta, \epsilon, \mathbf{q})|^2 + |f_{\downarrow\uparrow}(\eta, \epsilon, \mathbf{q})|^2. \quad (2d)$$

Here the sum over η is a multiple sum over electron states. It effectively sums over allowed electron-hole pairs of energy ϵ , wave vector \mathbf{q} , and the required spin combination. The flip intensities contain all, and nothing but, excitations leading to Stoner electron-hole pairs, $F^{\uparrow}(\epsilon, \mathbf{q})$ comprising those of minority-hole, majority-electron character, and $F^{\downarrow}(\epsilon, \mathbf{q})$ comprising those of majority-hole, minority-electron character. If all the

exchange-scattering amplitudes were the same magnitude, then the two flip intensities would correspond precisely to the two Stoner densities of states. The nonflip intensities contain all the direct scattering, some exchange scattering, and interference terms between the two. When $\mathbf{q} \approx 0$, then the direct-scattering terms will also include a large contribution from the dipole scattering mechanism.

It is clear from the definitions in Eq. (1) that the spin polarization of the incident and scattered electron beams must be measured in order to isolate the flip intensities. The geometry of an experiment designed to do this is illustrated in the inset in Fig. 1. The x axis is normal to the sample surface and the z axis is parallel to the majority orientation of the spins in the sample, \mathbf{S} , and lies in the plane of the surface. The xz plane also defines the scattering plane. An electron beam with longitudinal spin polarization \mathbf{P}_0 is incident at an angle θ to the x axis. The electrons scattered through an angle of 90° are collected and have spin polarization \mathbf{P}_f . Elastic scattering would redirect the incident electrons into the specularly reflected beam [or a higher-order low-energy electron diffraction (LEED) beam]. Inelastic scattering will cause some electrons to emerge at an angle $\alpha = 2\theta - \pi/2$ to the specularly scattered beam, where they are detected. The momentum change necessary to redirect an electron from the specularly scattered beam into the inelastically scattered beam is

$$q_x = (2mE/\hbar^2)^{1/2} (\sqrt{1 - \epsilon/E} \sin\theta - \cos\theta), \quad (3a)$$

$$q_z = (2mE/\hbar^2)^{1/2} (\sqrt{1 - \epsilon/E} \cos\theta - \sin\theta). \quad (3b)$$

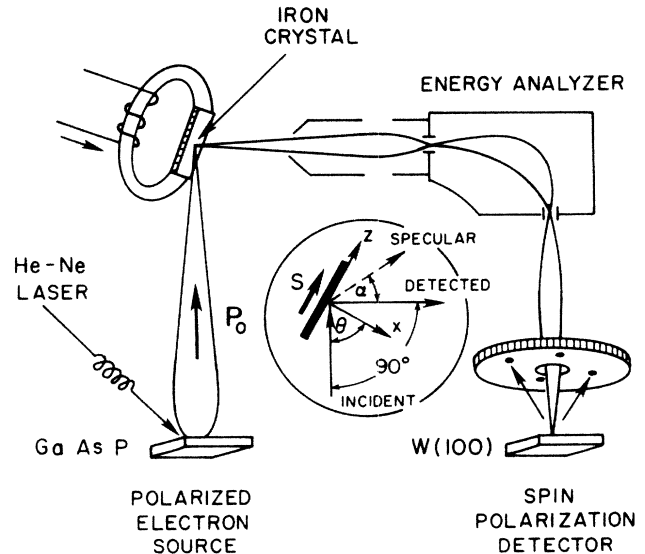


FIG. 1. Schematic picture of the apparatus. Electrons with spin-polarization \mathbf{P}_0 are extracted from a GaAsP cathode and scattered from the iron crystal. Electrons scattered by 90° pass through an energy analyzer and into the spin analyzer. The illustrated electron trajectory is distorted for clarity; in reality the electrons are directed into the page as they emerge from the energy analyzer. The inset illustrates details of the scattering geometry.

Assuming that multiple inelastic scattering is negligible, the component q_z must be absorbed by an excitation of the metal, in this case, by the creation of a single electron-hole pair with momentum q_z parallel to the surface. The component of momentum normal to the surface, q_x , may be provided by an excitation, by the surface itself, or by a combination of the two. Thus, in

principle, the experiment cannot distinguish between the creation of electron-hole pairs with different q_x if they have the same total energy and parallel momentum q_z .

To separate the different scattering channels, first consider the simplified case where \mathbf{P}_0 and \mathbf{S} are both parallel to the z axis. Then the z component of the final-state spin polarization is defined by

$$P_{fz}^s = \frac{(e \text{ detected with } \sigma \text{ along } S) - (e \text{ detected with } \sigma \text{ opposite } S)}{(e \text{ detected with } \sigma \text{ along } S) + (e \text{ detected with } \sigma \text{ opposite } S)}, \quad (4)$$

where $s = +$ or $-$ for \mathbf{P}_0 directed parallel or antiparallel to \mathbf{S} . It is also useful to define the "intensity asymmetry," $A(\epsilon, \mathbf{q})$:

$$A = \frac{(e \text{ detected when } P_0 \text{ along } S) - (e \text{ detected when } P_0 \text{ opposite } S)}{(e \text{ detected when } P_0 \text{ along } S) + (e \text{ detected when } P_0 \text{ opposite } S)}. \quad (5)$$

For the special case of a completely polarized incident beam, $|P_{0z}| = 1$, the application of Eq. (1) to these definitions gives

$$P_{fz}^+ = (N^\uparrow - F^\uparrow) / (N^\uparrow + F^\uparrow), \quad (6a)$$

$$P_{fz}^- = (N^\downarrow - F^\downarrow) / (N^\downarrow + F^\downarrow), \quad (6b)$$

$$A = [(N^\uparrow + F^\uparrow) - (N^\downarrow + F^\downarrow)] / J, \quad (6c)$$

$$J = N^\uparrow + F^\uparrow + N^\downarrow + F^\downarrow, \quad (6d)$$

where the explicit dependence on ϵ and \mathbf{q} has been suppressed.

If $|P_{0z}| \neq 1$, then the incident beam may be decomposed into a spin-up component of intensity $(1 + P_{0z})/2$ and a spin-down component of intensity $(1 - P_{0z})/2$. Use of Eqs. (4)–(6) for this composite beam gives

$$P_{fz}^\pm = [(N^\uparrow - F^\uparrow - N^\downarrow + F^\downarrow) + |P_{0z}| (N^\uparrow - F^\uparrow + N^\downarrow - F^\downarrow)] / [J(1 + A)] \quad (7a)$$

where

$$A = |P_{0z}| (N^\uparrow + F^\uparrow - N^\downarrow - F^\downarrow) / J. \quad (7b)$$

Letting $|P_{0z}| \rightarrow -|P_{0z}|$ in Eqs. (7a) and (7b) yields P_{fz}^- . A final correction must be made for the efficiency, D , of the spin detector. This is accomplished by dividing the left-hand side of Eq. (7a) by D so that the quantities P_{fz}^s represent the measured spin polarization. Then it is simple to solve for the four normalized scattering intensities

$$F^\uparrow / J = (1 - \beta_1 - \beta_2 + \beta_3) / 4, \quad (8a)$$

$$F^\downarrow / J = (1 + \beta_1 - \beta_2 - \beta_3) / 4, \quad (8b)$$

$$N^\uparrow / J = (1 + \beta_1 + \beta_2 + \beta_3) / 4, \quad (8c)$$

$$N^\downarrow / J = (1 - \beta_1 + \beta_2 - \beta_3) / 4, \quad (8d)$$

where

$$\beta_1 = [(1 + A)P_{fz}^+ + (1 - A)P_{fz}^-] / (2D),$$

$$\beta_2 = [(1 + A)P_{fz}^+ - (1 - A)P_{fz}^-] / (2|P_{0z}|D),$$

$$\beta_3 = A / |P_{0z}|.$$

The absolute intensities are recovered by multiplying by the measured total intensity of the energy-loss spectrum at this value of ϵ and \mathbf{q} .

For the general case of \mathbf{P}_0 and the surface normal subtending an angle θ , the full calculation must be performed in the four-dimensional product spin space of the incident electron and the target electron.²³ In the present case, this calculation gives precisely Eq. (8) for the z component of the spin polarization and the intensity asymmetry, with the understanding that

$$P_{0z} = P_0 \sin \theta. \quad (9)$$

Thus the spin-flip intensity spectra may be obtained from the experimental EELS spectrum and the spin-polarization data without making any model-dependent assumptions. The component of final-state spin polarization along the surface normal, P_{fx}^s , is

$$(1 + A)P_{fx}^+ = -(1 - A)P_{fx}^- = 2|P_{0x}|X/J \quad (10a)$$

where

$$X = \sum_{\eta} \text{Re}\{f_{\uparrow\uparrow}^*(\eta, \epsilon, \mathbf{q})[f_{\uparrow\uparrow}(\eta, \epsilon, \mathbf{q}) - g_{\uparrow\uparrow}(\eta, \epsilon, \mathbf{q})]\} + \text{Re}\{f_{\uparrow\downarrow}^*(\eta, \epsilon, \mathbf{q})[f_{\uparrow\downarrow}(\eta, \epsilon, \mathbf{q}) - g_{\uparrow\downarrow}(\eta, \epsilon, \mathbf{q})]\}. \quad (10b)$$

This component contains complicated interference terms between many direct- and exchange-scattering amplitudes. The sum over η makes it impossible to retrieve any phase information about the individual scattering amplitudes without a detailed knowledge of the band structure, wave functions, and scattering matrix elements.

III. EXPERIMENT

A. Apparatus

The four main components of the apparatus are the source of spin-polarized electrons, the sample and sample holder, the electrostatic deflection-energy analyzer, and the spin-polarization detector. These are illustrated schematically in Fig. 1. The source of spin-polarized electrons is a single crystal of $\text{GaAs}_{0.6}\text{P}_{0.4}(100)$ which is illuminated by the light from a HeNe laser. This type of source has been known for over a decade²⁴ and its principles of operation have been described in detail.²⁵ Briefly, the photoelectrons created by the laser light result principally from direct optical transitions between the valence and conduction bands at the Γ point of the Brillouin zone. The photoelectrons do not have sufficient energy to escape from the crystal, so it is necessary to lower the work function by depositing cesium on the surface in the presence of oxygen. The crystal then has a negative affinity for electrons of this energy, and they may be extracted as an external current. If the light incident on the crystal is circularly polarized, the dipole selection rule for the relevant optical transition at Γ indicates that the photoelectrons have a spin polarization of 0.5. The contribution from secondary electrons and other optical transitions reduces the spin polarization of the total extracted photocurrent.

A Pockels cell is used to switch the laser light between circular polarizations with positive and negative helicity, thus modulating the sign of the electron-spin polarization. A deflection-energy analyzer may be used to produce a monoenergetic beam of electrons, but this severely reduces the output current. An alternative method is to adjust the electron affinity so that only electrons within a narrow range of energies can escape from the crystal.²⁶ In this way, a current of 1.0–25 μA with an energy width of a few tenths of an eV and a primary energy of 22 eV can be delivered to the sample. Since the Stoner spectrum is a continuum, and since the exchange splitting of the bands in the iron sample is approximately 2 eV, a more monoenergetic source beam is not essential. A series of lenses accelerates the longitudinally spin-polarized photoelectrons and focuses them onto the sample.

The sample is a single crystal of iron cut to expose the (110) surface plane. It was cleaned by cycles of sputtering with Kr^+ ions, flashing to $\sim 600^\circ\text{C}$, and occasional heating in oxygen.²⁷ Cleanliness was monitored using Auger-electron analysis. The $\langle 110 \rangle$ surface normal and the $\langle 001 \rangle$ axis of easy magnetization correspond to the x and z directions in the inset of Fig. 1 and define the scattering plane of the electrons. This geometry has been chosen to minimize the effects of spin-orbit coupling. Spin-orbit coupling of the electronic states in iron may cause the electrons scattered elastically from the surface to be spin polarized, thus mimicking spin-flip events due to exchange scattering. Since the scattering plane is a crystal mirror-symmetry plane, this effect will not produce an intensity asymmetry. It may, however, alter the components of the spin polarization of the scattered electron beam in the mirror plane.²⁸ Because iron has a rather low atomic number, this latter effect is ex-

pected to be negligible. This is confirmed experimentally in Sec. III B. The sample is bound to a toroidal iron yoke, which forms the core of a transformer. By passing a current pulse through the transformer wiring, the sample can be remanently magnetized either parallel or antiparallel to the [001] direction. The torus forms a closed circuit for the magnetic flux lines, so that the low-energy electron beams are not deflected appreciably by the magnetic fields. The angle, θ , between the incident electron beam and the surface normal may be altered by rotation of the rotary feedthrough upon which the sample is mounted.

Electrons which are scattered at right angles to the incident electron beam (independent of θ) enter a transport lens and are focused onto the entrance of a cylindrical mirror deflection-energy analyzer. Those electrons having a particular kinetic energy form an image on the exit aperture and pass into the spin-polarization detector. The energy analyzer floats on a bias potential which is swept so that the electrons with different kinetic energies relative to the vacuum will be imaged on the exit slit in turn, recording a full spectrum as a function of energy loss.

In the spin-polarization detector,²⁹ the monoenergetic electron beam is first accelerated to a kinetic energy of 104.5 eV and then directed normally onto the (001) plane of a tungsten single crystal. The backscattered electrons are retarded and strike a channel-plate multiplier. The amplified current pulses resulting from the electrons then fall upon a position-sensitive resistance plate, and the spatial coordinates of each pulse are determined.³⁰ The pulses are displayed on an oscilloscope screen, as indicated at the bottom of Fig. 1, resulting in the LEED pattern from the (001) plane of tungsten. The intensity scattered into the LEED spots is sensitive to the spin of the incident electrons because of the effects of spin-orbit coupling on the reflection coefficient from tungsten. The tungsten crystal is oriented so that the intensity asymmetry between the (2,0) and $(\bar{2},0)$ spots measures the component of spin polarization parallel to the initial spin polarization \mathbf{P}_0 , and the (0,2) and $(0,\bar{2})$ spots measure the component perpendicular to \mathbf{P}_0 , but within the scattering plane. A simple transformation recovers the components along x and z which are required for the analysis. To collect a spin-polarization distribution, those counts occurring in windows about the (2,0) family of LEED spots are recorded as a function of the bias potential applied to the energy analyzer. The electron-energy-loss spectrum is then given by the sum of all the counts occurring in the (2,0) family of spots.

A total of 16 spectra must be accumulated to complete a set of measurements at a given scattering angle. For a given direction of sample magnetization, and for each of the two signs of \mathbf{P}_0 , the counts in four LEED spots are recorded simultaneously. These measurements are interleaved in time by modulating the light helicity with the Pockels cell. If the spin-polarization detector had no inherent asymmetry, or "baseline," then these data would be sufficient to determine the scattering intensities in the four channels with Eq. (8). In order to correct for the detector asymmetry, the measurements

are repeated with the sample magnetization reversed. Since only a minority of the electrons are scattered into the (2,0) family of LEED spots in the spin-polarization detector, the signal levels for these experiments are much lower than for conventional EELS. As a result, resolution must be sacrificed. The aperture in the transport lens accepts electrons with trajectories $\pm 3.0^\circ$ from right-angle scattering (i.e., $\pm 1.5^\circ$ in θ) and the overall energy resolution of the energy analyzer and the electron source is 0.4 eV full width at half maximum (FWHM). Under these conditions, the count rates are ~ 500 cps per LEED spot, and a complete set of spectra for one sample magnetization requires 5–6 h. It is therefore important to work at low pressures ($< 10^{-10}$ mbar), and to interrupt the experiment to clean the sample every 2–3 h. The detector crystal is cleaned every 20–30 min by flashing.

B. Data reduction

Measurements were performed at seven angles in the range $45^\circ < \theta < 70^\circ$, corresponding to a scattered beam emerging with $0^\circ < \alpha < 50^\circ$ from the direction of specular reflection. Figure 2 presents detailed results for $\theta = 60^\circ$. For this angle, $q_z = -0.95 \text{ \AA}^{-1}$. The electron-energy-loss spectrum is shown in Fig. 2(a). It is essentially the

same as that presented earlier by Kirschner,¹⁶ except that it extends down to loss energies of 7 eV. The existence of a large, diffuse, elastic peak indicates the presence of some surface disorder. This probably results from the fact that the iron crystal was annealed a minimal amount after sputtering for fear of bringing impurities to the surface.²⁷ Most importantly, the spectrum confirms the existence of a broad peak at a loss energy of ~ 2 eV superimposed on a continuum of excitations.

The intensity asymmetry as a function of loss energy is presented in Fig. 2(b). The left-hand scale is the measured asymmetry, and the right-hand scale indicates what the asymmetry would be if $|P_{0z}|$ were unity. A peak in the intensity asymmetry coincides with that which occurs in the energy-loss spectrum. Figure 2(b) also presents the z components of the spin polarization P_{fz}^s for P_{0z} parallel ($s = +$) and antiparallel ($s = -$) to S . The competition between the direct and exchange scattering can be followed here as the loss energy changes. At very low loss energy the states available in phase space for the creation of electron-hole pairs shrinks to the Fermi surface as $\epsilon \rightarrow 0$. In the limit of elastic scattering, no excitations are possible and the exchange scattering contribution must vanish. Since only direct scattering is possible, the initial and final spin po-

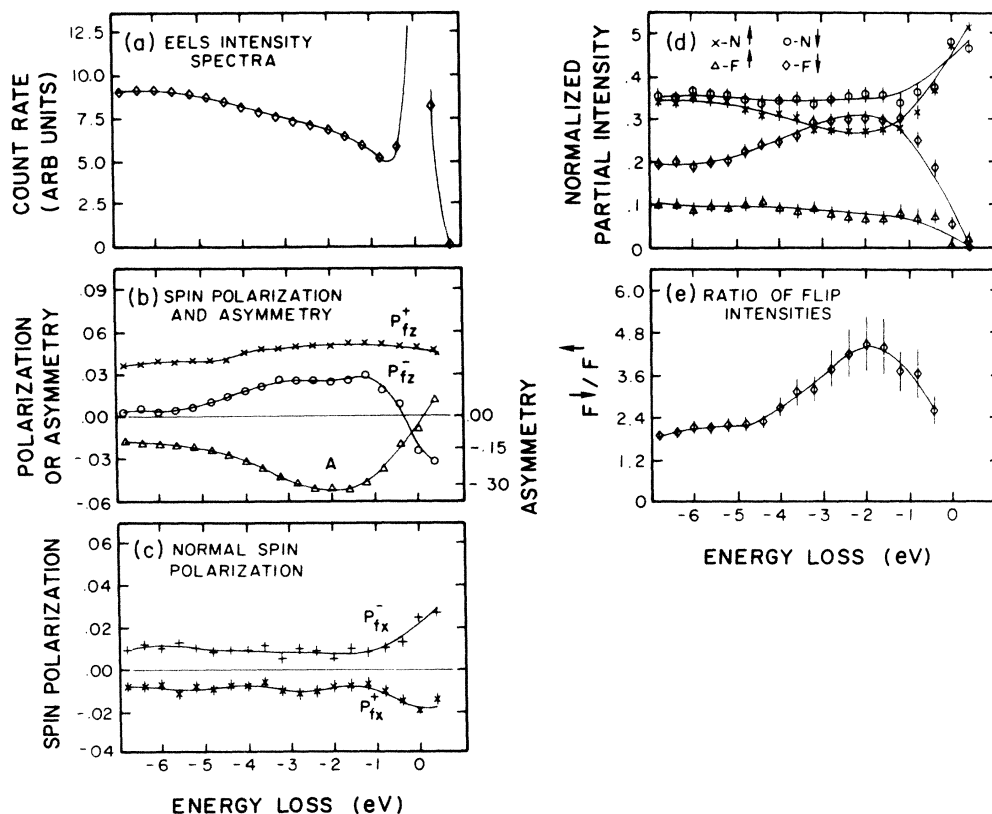


FIG. 2. Sample data analysis for $\theta = 60^\circ$. (a) The EELS intensity spectrum. (b) The spin polarization along z when the spin polarization of the incident beam has a component parallel ($s = +$) and antiparallel ($s = -$) to the majority-spin direction in the sample. The intensity asymmetry, with right-hand scale corrected for $|P_{0z}| = 1$, is also shown. (c) The spin polarization along the surface normal, \times . (d) Relative scattering intensities in the four scattering channels. (e) Ratio of the flip intensities.

larizations are approximately the same. Thus the spin polarization for $s = +$ and $s = -$ at $\epsilon = 0$ differ effectively in sign only. At larger energy loss there is a dramatic change in P_{fz}^- as exchange scattering becomes important. When $s = -$, most exchange events add an electron polarized along $+z$ to the scattered beam and remove one polarized nominally along $-z$, and the net spin polarization therefore becomes more positive. On the other hand, P_{fz}^+ changes little since the incoming electrons already have spins directed nominally along $+z$. At even larger values of loss energy, below the exchange splitting of ~ 2 eV, P_{fz}^- becomes more negative again as the large density of states within the d bands is no longer available for exchange scattering.

The results in Fig. 2(b) can be used to calibrate $|\mathbf{P}_0|$. Since F^+ and $F^+ \rightarrow 0$ as $\epsilon \rightarrow 0$, Eq. (8) yields $\beta_1 = \beta_2$ and $\beta_3 = 1$. These two equations yield the product and quotient of $|\mathbf{P}_0|$ and the detector efficiency D , and these may therefore be determined, in principle, from the measured spin polarization and intensity asymmetry at $\epsilon = 0$. In reality, the equation for $D/|\mathbf{P}_0|$ involves the quotient of small numbers determined from the difference of large numbers, and is very unstable with respect to small measurement errors. The second equation is insensitive to experimental error and yields

$$[(1+A)P_{fz}^+ - (1-A)P_{fz}^-]_{\epsilon=0} = 2D |\mathbf{P}_0| \sin\theta. \quad (11)$$

Since the intensity asymmetry at $\epsilon = 0$ is small at a primary beam energy of 22 eV,²⁷ it may be neglected in comparison to unity. Knowing the detector efficiency³¹ as $D = -0.25$, it is possible to determine the initial spin polarization. In the present experiments, the data yield $|\mathbf{P}_0| = 0.20 \pm 0.02$ after averaging over all angles. This is much lower than the $|\mathbf{P}_0| = 0.35$ expected from a GaAsP source.^{24,26} This discrepancy could be due to sputtering the GaAsP crystal,³² the use of elliptically (as opposed to circularly) polarized light, saturation of the channel plate by the large count rate in the diffuse elastic peak, or contamination of the detector crystal. By operating the electron source at low current, so that the channel plates did not saturate in the elastic peak, it was found that saturation caused the spin polarization to be slightly underestimated by a factor which falls within the 2% standard deviation quoted above. An adjustment of this size has little effect on the subsequent results. The light polarization and the cleanliness of the detector crystal were checked and found to be satisfactory. The low value of the source polarization is therefore attributed to the effects of saturation and of cleaning the GaAsP crystal by sputtering and heating. The data have been analyzed by using the value of $|\mathbf{P}_0|$ determined using Eq. (11) for each data set.

The spin-polarization components along the surface normal, x , are shown in Fig. 2(c). These are plotted as $(1+A)P_{fx}^+$ and $(1-A)P_{fx}^-$ to allow comparison with Eq. (10a). In contrast to the components along z , these do not show any clear structure. This is to be expected since they result from the interference of many scattering amplitudes. The fact that, to a good approximation, the two curves are equal in magnitude and opposite in

sign, is a confirmation of the analysis procedure. If it is assumed that diffuse elastic scattering and specular elastic scattering are affected in the same way by spin-orbit coupling, then the absence of spin-orbit-coupling effects in the data can be inferred by comparing the measured spin polarization at $\epsilon = 0$ in Figs. 2(c) and 2(d). In the present geometry, spin-orbit coupling of the electronic states of iron may rotate and rescale the spin polarization of the elastically scattered beam with respect to \mathbf{P}_0 .³³ The rotation by spin-orbit coupling must be small since the experimental ratio P_{fz}^s/P_{fx}^s at $\epsilon = 0$ closely approximates $P_{0z}/P_{0x} = \tan\theta$. The average rotation for the seven data sets is $\delta\theta = -2^\circ \pm 2^\circ$, which is of the order of the angular resolution of the apparatus. The small size of the rotation implies an upper limit of a few percent on the rescaling of the magnitude of the incident spin polarization. This supports the calibration procedure for $|\mathbf{P}_0|$ carried out above.

Finally, the relative intensities in the four scattering channels are shown in Fig. 2(d). The flip intensities correspond to Stoner electron-hole pairs. F^+/J corresponds to majority holes and minority electrons. The curve shows unambiguously that the broad feature in the energy-loss spectrum and intensity asymmetry are due to excitations of this type. The peak occurs because the Fermi level lies between majority and minority d bands derived from the same paramagnetic band, and a large number of electron-hole excitations of the appropriate spin character are thus possible. The F^+/J events, on the other hand, have a rather flat spectrum. These Stoner excitations involve minority holes and majority electrons, and cannot be formed by excitations between exchange-split bands arising from the same paramagnetic band. They represent, principally, excitations with holes in d bands and electrons in sp bands. Since the density of states for sp bands is not localized in energy, neither is the intensity in this channel.

The nonflip intensities involve both direct and exchange scattering between electrons of like spin, as well as direct scattering between electrons of unlike spin. The final state in both processes is an electron-hole pair with like spins. The nonflip intensities are seen to be generally larger than the flip intensities. This results from the fact that direct scattering involves a much smaller energy and momentum transfer than exchange scattering, and is therefore expected to have a greater amplitude. Two observations are helpful in understanding some qualitative features of the nonflip intensities. First, reference to the spin-resolved density of states for iron² shows that there are many more configurations which have an electron-hole pair within the spin-down subsystem than there are within the spin-up subsystem. The scattering amplitudes $f_{\uparrow\uparrow}$, $f_{\uparrow\downarrow}$, and $g_{\uparrow\uparrow}$ should therefore dominate the nonflip intensities in Eq. (2). Second, the direct-scattering processes given by the amplitudes $f_{\uparrow\uparrow}$ and $f_{\uparrow\downarrow}$ differ only in the spin of the states of the incoming electron. Since these are direct processes, these electrons lose only a small fraction of their energy and reemerge from the crystal. The electronic states at these high energies (15–22 eV above the Fermi level) are predominantly sp -like in iron and have a smaller ex-

change splitting than the d bands.³⁴ For the purposes of a qualitative argument, this exchange splitting may be neglected. This implies that the two direct-scattering amplitudes $f_{\uparrow\uparrow}$ and $f_{\uparrow\downarrow}$ should have similar magnitudes. The similarity of the intensities in the two nonflip channels may therefore be seen as a result of the dominance of these two direct-scattering processes. Since nonflip exchange scattering within the spin-down subsystem can create excitations only via the scattering amplitude $g_{\downarrow\downarrow}$, it contributes only to the N^{\downarrow}/J channel. This is consistent with the fact that $N^{\downarrow}/J > N^{\uparrow}/J$ in the energy-loss range governed by excitations within the d bands. While these arguments based on the density of states for certain types of final states are appealing, they take no account of the effects of interference between direct and interchange scattering. More information is needed to determine the various contributions to the nonflip intensities with certainty.

Penn³⁵ has attempted an approximate separation of the scattering mechanisms by applying a simplified model to the spin-resolved EELS data published by Kirschner.¹⁶ He comes to conclusions which are in disagreement with the above interpretation of the spin-resolved, relative scattering intensities; that is, he concludes that exchange scattering in the sp bands is the dominant scattering mechanism, and that it is much larger than both spin-flip, exchange scattering in the d bands and direct scattering. The model Penn has used for this analysis is based on the same type of assumptions as those used for the qualitative discussion in the present work, but he has taken each assumption a step further and applied it to a quantitative evaluation. Thus he assumes that the exchange splitting for the sp bands is negligible at *all* energies. By using this assumption, Penn obtains an exact cancellation of terms in the exchange scattering in the sp bands, and is able to identify the exchange scattering in the d -band states near the Fermi level. However, while the neglect of the exchange splitting of the sp bands is, perhaps, allowable for the direct scattering between electronic states of high energy, spin-polarized band-structure calculations³⁴ show that it is not valid when the final states are near the Fermi level, as is the case for exchange scattering. Thus, Penn's separation of the sp - and d -band contributions to the exchange scattering is questionable. Next, he assumes that there are no majority d -band states above the Fermi level. This is correct for a saturated itinerant-electron ferromagnet, such as nickel, but not for an unsaturated ferromagnet such as iron. Taken together, these assumptions are certain to misrepresent the relative importance of the sp - and d -band exchange scattering, although it is not clear to what extent the use of a more realistic band structure would modify Penn's conclusions.

There is a further uncertainty in Penn's analysis. He has apparently obtained the data he analyzed by digitizing the curves published in Ref. 16, and this has unfortunately introduced considerable numerical uncertainty. This uncertainty is compounded when the differences and ratios of the digitized quantities are formed, and has led to the presentation of "data" which is at odds with

the original data. This is most evident in Fig. 3 of Ref. 35. This figure shows that the ratio of flip intensities, $F^{\downarrow}/F^{\uparrow}$, is essentially independent of loss energy, whereas the original data reveal a clear peak in this quantity near a loss energy of 2 eV. This peak is evident in the present data as well [see Fig. 2(e)], where it is even more pronounced. The existence of such a peak proves that Stoner excitations are most numerous within a range of energy loss characteristic of the exchange splitting of the d bands. This is to be expected, since the density of states in the d bands is far greater than that in the sp bands. While Penn has properly brought attention to the possible importance of free-electron-like Stoner excitations in ferromagnets, it seems clear that Stoner excitations in the d bands play the major role in these experiments.

IV. DISCUSSION

A. General

The experimental results are presented in Fig. 3 for the seven values of θ that were investigated. The energy-loss spectra and relative scattering intensities in all four channels are shown. The interpolating lines are weighted, cubic splines. The former have been corrected by a factor of $\tan\theta$ to compensate for the variation in the incident electron flux and spectrometer acceptance area as the angle is changed. Before considering a detailed analysis of the Stoner spectra, several aspects of the data set as a whole deserve comment.

The first point concerns the change in the shape of the energy-loss spectrum as the angle θ is increased. In specular reflection ($\theta=45^\circ$) the contribution from the dipole scattering mechanism is very large, and a pole at $\epsilon=0$ in the kinematic prefactor in the expression for the dipole scattering cross section²⁰ causes the spectrum to increase monotonically as ϵ decreases. As θ is increased, the total cross section falls quickly as the electrons no longer interact with the dipole lobe of the long-range electric fields. Since the lobe has an angular width $\gamma \approx \epsilon/2E$, this condition is met for different $\epsilon=\epsilon_0$ in the spectra collected at different values of $\alpha=2\theta-\pi/2$. For the data taken with $\theta=47.5^\circ$ ($\alpha=5^\circ$), $\epsilon_0=2.8$ eV. Thus the scattering cross section is greatly reduced close to the elastic peak, but is reduced less at energies $\epsilon > \epsilon_0$ because dipole scattering is still effective. This results in a broad peak in the spectrum at $\epsilon \sim \epsilon_0$. The peak moves to larger energy loss for $\theta=50^\circ$ ($\epsilon_0=5.7$ eV), and moves off the recorded spectrum for $\theta > 55^\circ$. The very gradual fall in the energy-loss spectrum which occurs at large loss energies when $\theta > 55^\circ$ is likely due to the transmission function of the electron lenses. The dependence of the width of the dipole lobe on loss energy affects even the specular data. The smallest loss energy which can be resolved is ≈ 0.4 eV, and this corresponds to the value of ϵ_0 for the angle $\alpha=0.7^\circ$. Dipole scattering at greater angles does not contribute to the cross section at 0.4 eV loss energy. Since the acceptance angle of the transport lens is $\pm 3^\circ$ in α , the outer annulus of the specularly scattered electron beam cannot contribute dipole scattering in this energy range. At energy losses $\epsilon > 1.6$ eV, how-

ever, dipole scattering from the entire beam can contribute to the cross section. This creates the small hump in the spectrum at approximately this energy. In data taken with greater angular resolution, and a smaller primary beam energy,¹⁷ this hump moves much closer to the elastic peak and cannot be resolved in the specular data.

It is also interesting to note the behavior of the intensity asymmetry as a function of the scattering angle. Because the experiment is spin polarized, the intensity asymmetry in the flip and nonflip channels alone can be determined in addition to the total intensity asymmetry. This allows some insight into the physical origin of the

intensity asymmetry. Two different mechanisms involving exchange scattering have been proposed to account for the asymmetry. Although these proposals refer specifically to experiments involving the scattering of spin-polarized electrons from nickel,¹¹ the basic ideas should apply equally well to the present experiments using iron.

Mills¹⁴ is particularly interested in the specular scattering geometry, and suggests that, under these conditions, the intensity asymmetry might occur principally in the nonflip channels. He proposes an "interference model" which stresses the role of the surface in EELS. In this model, surface dipole scattering is the main

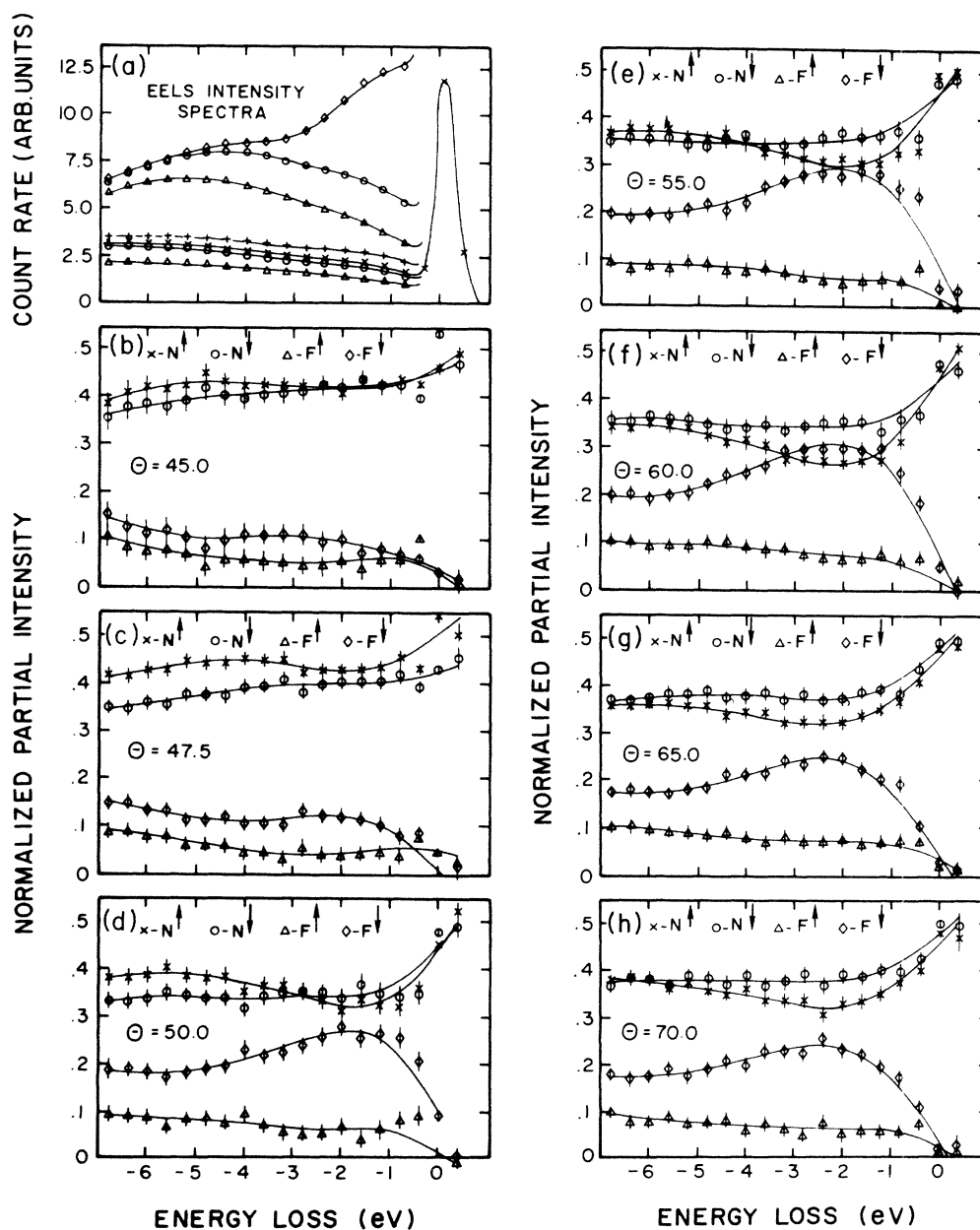


FIG. 3. Summary of the spin-polarized EELS data. (a) The intensity spectra for (from top to bottom) $\theta = 45^\circ, 47.5^\circ, 50^\circ, 55^\circ, 60^\circ, 65^\circ,$ and 70° . (b)–(h) The relative scattering intensities in the four scattering channels for the indicated angles θ .

direct-scattering mechanism, and exchange scattering is provided by a local exchange potential. He suggests that the intensity asymmetry would then arise because the sign of the interference between the direct dipole scattering and the exchange scattering in the *nonflip* channels of Eqs. (2c) and (2d) would reverse when \mathbf{P}_0 is reversed. He argues that Stoner excitations must play an insignificant role in the specular geometry, since, as in neutron scattering, the cross section for magnetic excitations near $\mathbf{q}=0$ is taken up entirely by spin waves. Vignale and Singwi,¹⁵ on the other hand, emphasize the calculation of the excitation cross section in the bulk in their analysis. They find that the exchange scattering of electrons is formally identical to neutron scattering only if the electron momenta are much greater than the Fermi momentum. For small primary momenta, such as those used in the present experiments, they conclude that electron scattering can couple to both spin waves and Stoner excitations near $\mathbf{q}=0$ with comparable cross sections. Using a simplified, rigidly split model of the electronic bands, they find an intensity asymmetry in the flip channels due to Stoner excitations at $\mathbf{q}=0$. For excitations of large \mathbf{q} , corresponding to nonspecular scattering, Stoner excitations are found to dominate.

The intensity asymmetries for the present data for angles near specular are presented in Fig. 4. At large angles, the great majority of the intensity asymmetry is in the flip channels, and is centered in the energy-loss range corresponding to electron-hole excitations in the *d* bands. There is, therefore, no question that exchange scattering leading to Stoner electron-hole pairs is the dominant mechanism at large angles. At smaller angles ($\theta=45^\circ$ and 47.5°), where Mill's arguments apply, the total intensity asymmetry is 5 or 6 times smaller, and the intensity asymmetry in the flip and nonflip channels is comparable in magnitude. The asymmetry observed in the nonflip channels in iron may well be due to the interference mechanism proposed by Mills. The data are suggestive of the following interpretation. As was discussed in Sec. III, little intensity asymmetry is expected due to differences in the direct-scattering intensities. This is especially true at $\alpha=0$, where dipole scattering dominates the process. Because of the few unoccupied states in the majority *d* bands, it is also expected that the nonflip exchange-scattering term $|g_{\uparrow\uparrow}|^2 - |g_{\downarrow\downarrow}|^2$ will be negative. The positive nonflip intensity asymmetry at small angles is therefore likely due to the interference term, which has been brought into prominence by the large cross section for dipole scattering at small angles. As the scattering angle increases, the nonflip intensity asymmetry decreases since the dipole scattering in the interference term is reduced. The positive nonflip intensity asymmetry persists at large energy loss until $\theta \approx 55^\circ$, since the dipole scattering continues to contribute only at large loss energies [recall Fig. 3(a)]. In the limit of $\theta \geq 55^\circ$, all that remains of the nonflip intensity asymmetry is a negative contribution centered at an energy corresponding to excitations within the *d* bands. This asymmetry is attributed to the difference $|g_{\uparrow\uparrow}|^2 - |g_{\downarrow\downarrow}|^2$. With this interpretation in mind, it is possible to trace the development of this negative peak

through the sequence of nonflip intensity asymmetry curves for smaller angles.

The intensity asymmetry which appears in the flip channels at $\alpha \approx 0$ cannot arise from interference effects, and must represent exchange scattering from magnetic excitations. Its presence in the specular beam is in agreement with the conclusion of Vignale and Singwi that Stoner excitations should have a reasonable cross section even at $\mathbf{q}=0$ (if spin waves were present, the experiment would not be able to resolve them). The flip intensity asymmetry has a negative sign, as is expected, but shows little structure at an energy near the exchange

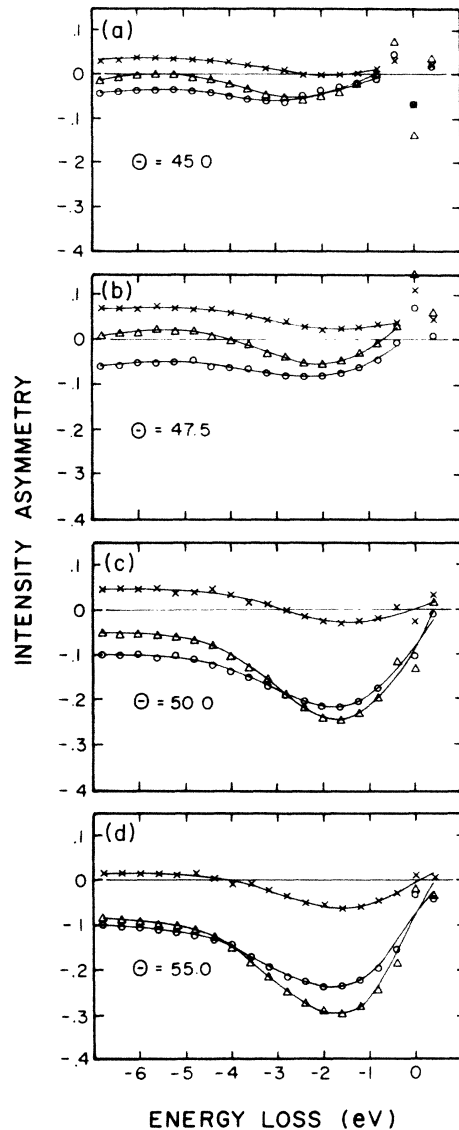


FIG. 4. Partial and total intensity asymmetries, corrected for $|P_{0z}|=1$, for the indicated values of θ . \times is the nonflip intensity asymmetry $(N^{\uparrow}-N^{\downarrow})/J$; \circ is the flip intensity asymmetry $(F^{\uparrow}-F^{\downarrow})/J$; \triangle is the total intensity asymmetry $(N^{\uparrow}+F^{\uparrow}-N^{\downarrow}-F^{\downarrow})/J$. The data close to $\epsilon=0$ for $\theta=45^\circ$ and 47.5° are unreliable because of saturation of the electron counter.

splitting. This is a consequence of the fact that F^1/J shows no strong peak in Fig. 3 at small angles. This somewhat surprising result is consistent with previous studies for specular scattering from iron,¹⁷ which also show a small relative contribution from flip processes at specular scattering. The statistical noise in the much larger nonflip channels is probably large enough to hide structure in the flip channels. In summary, the flip and nonflip intensity asymmetries provide evidence that both exchange scattering from Stoner excitations, and the interference of direct and exchange scattering, give contributions to the intensity asymmetry in the specular beam.

B. Stoner densities of states

The partial intensities for flip events are related to the Stoner densities of states in a complicated way. The scattering amplitudes $g_{\sigma_i\sigma_f}(\eta, \epsilon, \mathbf{q})$ are dependent on the electron transmission coefficients at the surface, the penetration and escape depths of the electrons, and the matrix elements of the screened, electron-electron Coulomb interaction. The spin-resolved partial scattering intensities are given by summing over the many different electron-hole-pair combinations [see Eq. (2)] of a given total energy and crystal momentum. It is not surprising that no detailed model for evaluating these two-particle, exchange, impact scattering intensities in realistic ferromagnets has yet been developed. To make some progress in the data analysis, it is customary to assume that the sum over η "averages out" the details of these processes, and that the most important remaining determinant of the flip intensity spectrum is the number of distinct, allowed electron-hole pairs of a given energy, crystal momentum, and spin combination. This assumption is equivalent to assuming that all the individual scattering amplitudes are of equal magnitude. Under this assumption, Eqs. (2a) and (2b) reduce to a simple counting over allowed electron-hole final-state configurations; that is, to the Stoner density of states $\rho_{\sigma\sigma'}(\epsilon, \mathbf{q})$,²

$$\rho_{\sigma\sigma'}(\epsilon, \mathbf{q}) = (1/N) \sum_{n,m} \sum_k \{n(E_n)[1-n(E_m)]\} \times \delta(E_n(\mathbf{k}, \sigma) - E_m(\mathbf{k} + \mathbf{q}, \sigma') + \epsilon). \quad (12)$$

In this equation, m and n number the electronic bands which have the spin-dependent dispersion relation $E_n(\mathbf{q}, \sigma)$. The Fermi occupation factors $n(E)$ ensure that the states E_n and E_m are occupied and unoccupied, respectively.

Calculations of the Stoner densities of states for iron at zero temperature for various values of \mathbf{q} have been carried out by Cooke, Lynn, and Davis² and by Cooke.³⁶ These calculations are based on a self-consistent, ferromagnetic band structure presented in Ref. 2, in which the exchange splitting of each band is dependent upon both the energy and wave vector. Calculations of the spin-wave dispersion using this band structure have been shown to give excellent agreement with experimental

neutron scattering data.² Calculations of the Stoner density of states for majority holes and minority electrons, $\rho_{\uparrow\downarrow}(\epsilon, \mathbf{q})$, show a strong peak at the energy corresponding to the exchange splitting of the d bands. An example is shown in Fig. 5(a), for the crystal momentum $q_x = 0.78$ and $q_z = -0.95 \text{ \AA}^{-1}$. The density-of-states curve has been convolved with a Gaussian of FWHM = 0.4 eV to simulate the broadening due to the limited experimental resolution. The peak is very suggestive of that observed in the experimental partial intensity F^1/J appropriate to the creation of this type of Stoner excitation. The much smaller Stoner density of states for minority holes and majority electrons, $\rho_{\downarrow\uparrow}(\epsilon, \mathbf{q})$, is also shown. As expected, the latter does not show the peak associated with electron-hole pairs within the exchange-split d bands. This is in agreement with the small, structureless experimental curves for the partial intensity F^1/J . It therefore seems reasonable to attribute the gross features of the experimental flip intensities to the Stoner density of states, and to consider the effects of the scattering amplitudes as of secondary importance.

In order to try and understand the variation of the F^1/J partial intensity with scattering angle θ , $\rho_{\uparrow\downarrow}(\epsilon, \mathbf{q})$ was calculated for a sequence of \mathbf{q} along a line in reciprocal space given by the momentum difference between the scattered and incident electron beams at the experimental values of θ . Of course, only q_z [see Eq. (3a)] is strictly conserved in the EELS experiments be-

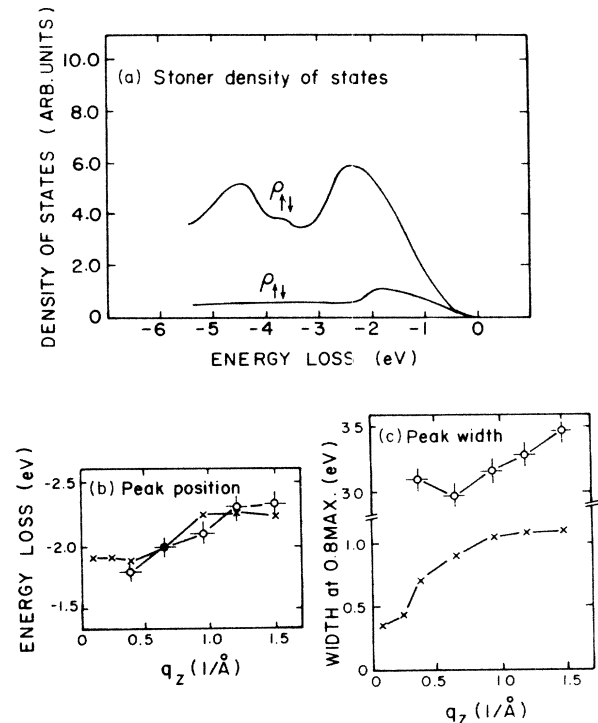


FIG. 5. A comparison of the Stoner densities of states and the measured F^1/J . (a) Stoner density of states for $q_z = -0.95$, $q_x = 0.78 \text{ \AA}^{-1}$, corresponding to a scattering angle $\theta = 60^\circ$: $\rho_{\uparrow\downarrow}(\epsilon, \mathbf{q})$ is the majority hole-minority electron, $\rho_{\downarrow\uparrow}(\epsilon, \mathbf{q})$ is the minority hole-majority electron. (b) Position of the peak in $\rho_{\uparrow\downarrow}(\epsilon, \mathbf{q})$ (\times) and the measured F^1/J (\circ). (c) Full width at 0.8 maximum of $\rho_{\uparrow\downarrow}(\epsilon, \mathbf{q})$ (\times) and the measured F^1/J (\circ). Note the break in the scale.

cause the surface breaks the translational symmetry along the x direction. A better quantity for comparison to experiment might be the Stoner density of states $\rho_{11}(\epsilon, q_x)$, which has been integrated over q_x . Since calculations of this quantity are not available, q_x was chosen according to Eq. (3b), which neglects surface transmission effects. The Stoner density-of-states curves are similar to that in Fig. 5(a) (which corresponds to $\theta=60^\circ$), except that the magnitude, energetic position, and width of the major peak is dependent on q . The dispersion of this peak is illustrated in Fig. 5(b), and the variation of the peak width is shown in Fig. 5(c). The peak width was measured at 0.8 of the peak height, so that the measured width would not be affected by the "background" of excitations within the sp bands. As expected, the peak in the Stoner density of states become broader and moves to larger energy loss as the scattering angle (i.e., q) is increased. This is because, at small q , the electron and hole are nearly vertically displaced on an energy-band diagram. Thus, each pair has a total energy ϵ close to the exchange splitting. As q increases, the electrons and holes are gradually displaced more and more horizontally on the energy-band diagram, so that the possible final-state pairs sample both a greater range of total energy, and, due to dispersion of the bands, a larger average total energy.

The experimental peak positions and widths for F^1/J are also plotted on Figs. 5(a) and 5(b). Precisely the same trends are seen. At very small q ($\theta=45^\circ$ and 47.5°), no clear peak is evident in F^1/J in Fig. 3, even though the flip intensity asymmetry in Fig. 4 shows that a signal for flip events is present. This is probably because the flip events are obscured by the statistical fluctuations of the large number of dipole scattering nonflip events. At $\theta \geq 50^\circ$, a clear peak in F^1/J emerges and disperses to higher energy loss with increasing θ . This dispersion is of the correct size and momentum dependence to be associated with the shift in the Stoner density of states, and offers clear experimental verification of q -dependent structure in the Stoner continuum of iron. The experimental peak width also increases, but is always much greater than that of the peak in the Stoner density of states. This is consistent with all previous measurements of the Stoner excitation spectrum in iron,^{16,17} nickel,¹¹ and spin glasses,^{12,13} and suggests that the exchange splitting in these materials is less uniform than that found in the calculations. It may also be that matrix-element effects or an integration of the Stoner density of states over q_x might substantially broaden the peak in the calculation.

These results point out the need for more detailed theoretical calculations in order that the data can be more fully understood. An account of matrix-element effects in the Born approximation,¹⁵ using a realistic band structure, with the results summed appropriately along q normal to the surface,¹⁴ would be a most worthwhile undertaking.

V. CONCLUSIONS

The electron-hole excitations with different spin configurations have been separated and studied experi-

mentally in iron using spin-resolved EELS. The data were interpreted using the explicit two-particle scattering model of Yin and Tosatti, and analyzed in the 4×4 product spin space of the incident and target electrons. The detection of the energy loss, momentum change, and apparent reversal of spin of a scattered electron indicated the creation of a Stoner excitation in the metal. These spin-flip events were found to be very important in the off-specular, impact scattering regime, where they comprise up to one-third of the total electron-hole excitations and are responsible for the great majority of the observed intensity asymmetry. They were also detected under specular and near-specular scattering conditions, but their relative importance decreases compared to the strong dipole scattering. The intensity asymmetry of the specularly scattered beam is made of a portion due to two-particle exchange scattering, and a portion due to the interference between direct- and exchange-scattering amplitudes, as proposed by Mills. The observation of sizable effects from exchange, impact scattering at all angles indicates that, despite its theoretical complexity, this mechanism must be considered in the analysis of EELS experiments.

Stoner excitations of majority-hole-minority-electron character (F^1 events) were found to be much more likely than those of minority-hole-majority-electron character (F^1 events). This difference was especially pronounced at a loss energy of ~ 2 eV, where a broad peak occurs in the F^1 partial intensity. These results may be simply interpreted by reference to the Stoner densities of states of iron. The F^1 partial intensity is structureless because most of the available electron-hole pairs of appropriate spin are in quickly dispersing sp bands, and it is small because of the small number of majority electron states above the Fermi level. The F^1 partial intensity is larger because the number of neither electron nor hole states of appropriate spin is severely restricted. Structure in this flip intensity is due to excitations in the flat, exchange-split d bands near the Fermi energy, which result in a prominent peak in the Stoner density of states. At an energy loss corresponding to this exchange splitting, the F^1 partial intensity is dominated by Stoner excitations within the d bands.

As the crystal momentum of the Stoner excitation (i.e., the scattering angle) is increased, the peak in the F^1/J partial intensity becomes broader and shifts to larger loss energy. These trends are also observed in the peak in the Stoner density of states for minority-electron-majority-hole pairs within the d bands. The present experiments are the first measurement of its dispersion and represent significant progress toward a mapping of the spectrum of single-particle magnetic excitations within the Stoner continuum.

ACKNOWLEDGMENTS

We are grateful to J. F. Cooke for providing the calculations of the Stoner densities of states, and to J. Larscheid for technical assistance. D. V. wishes to acknowledge the financial support of the Natural Sciences and Engineering Research Council of Canada.

- *Present address: Physics Department, Indiana University, Bloomington, IN 47401.
- ¹C. Herring, in *Magnetism IV*, edited by G. T. Rado and H. Suhl (Academic, New York, 1966).
- ²J. F. Cooke, J. L. Lynn, and H. L. Davis, *Phys. Rev. B* **21**, 4118 (1980).
- ³F. Englert and M. M. Antonoff, *Physica* **30**, 429 (1964).
- ⁴H. A. Mook and R. M. Nicklow, *Phys. Rev. B* **1**, 336 (1973); J. W. Lynn, *ibid.* **11**, 2624 (1975); H. A. Mook and D. Tschetti, *Phys. Rev. Lett.* **43**, 2029 (1979).
- ⁵T. Moriya, *Spin Fluctuations in Itinerant Electron Magnetism* (Springer-Verlag, Berlin, 1985).
- ⁶Y. Ishikawa, Y. Noda, Y. J. Uemura, C. F. Majkrzak, and G. Shirane, *Phys. Rev. B* **31**, 5884 (1985).
- ⁷R. E. De Wames and L. A. Vredevoe, *Phys. Rev. Lett.* **18**, 853 (1967).
- ⁸E. D. Thompson, *Ann. Phys. (N.Y.)* **22**, 309 (1963).
- ⁹H. Ibach (private communication).
- ¹⁰S. Yin and E. Tosatti, International Centre for Theoretical Physics, Trieste, Report No. IC/81/129, 1981 (unpublished).
- ¹¹J. Kirschner, D. Rebenstorff, and H. Ibach, *Phys. Rev. Lett.* **53**, 698 (1984).
- ¹²H. Hopster, R. Raue, and R. Clauberg, *Phys. Rev. Lett.* **53**, 695 (1984).
- ¹³S. Modesti, F. Della Valle, R. Rosei, E. Tosatti, and J. Glazer, *Phys. Rev. B* **31**, 5471 (1985).
- ¹⁴D. L. Mills, *Phys. Rev. B* **34**, 6099 (1986).
- ¹⁵G. Vignale and K. S. Singwi, *Phys. Rev. B* **32**, 2824 (1985).
- ¹⁶J. Kirschner, *Phys. Rev. Lett.* **55**, 973 (1985).
- ¹⁷J. Kirschner and S. Suga, *Surf. Sci.* **178**, 327 (1986).
- ¹⁸H. Scheidt, M. Glöbl, V. Dose, and J. Kirschner, *Phys. Rev. Lett.* **51**, 1688 (1983); E. Kisker, K. Schröder, M. Campagna, and W. Gudat, *ibid.* **52**, 2285 (1984); J. Kirschner, *Solid State Commun.* **49**, 39 (1984).
- ¹⁹H. Ibach and D. L. Mills, *Electron Energy Loss Spectroscopy and Surface Vibrations* (Academic, New York, 1982).
- ²⁰D. L. Mills, *Surf. Sci.* **48**, 59 (1975).
- ²¹The term “exchange” scattering is used in this paper to describe events where the incident and detected electrons are not the same ones. While this is established usage, it risks confusion with scattering by the “exchange potential” in the Hartree-Fock sense. In a Hartree-Fock Formulation (Refs. 7 and 14) no distinction need be made, but when explicit two-particle scattering events are included (Ref. 10) exchange scattering is more general than scattering from the exchange potential.
- ²²C. H. Li, S. Y. Tong, and D. L. Mills, *Phys. Rev. B* **21**, 3057 (1980).
- ²³J. Kessler, *Polarized Electrons*, 2nd ed. (Springer-Verlag, Berlin, 1985).
- ²⁴E. Garwin, D. T. Pierce, and H. C. Siegmann, *Helv. Phys. Acta* **47**, 393 (1974); D. T. Pierce, R. J. Celotta, G.-C. Wang, W. N. Unertl, A. Galejs, C. E. Kuyatt, and S. R. Mielezarek, *Rev. Sci. Instrum.* **51**, 478 (1980).
- ²⁵M. Wölecke and G. Borstel, in *Optical Orientation*, edited by F. Meier and B. P. Zakharchenya (North-Holland, Amsterdam, 1984).
- ²⁶J. Kirschner, H.-P. Oepen, and H. Ibach, *Appl. Phys. A* **30**, 177 (1983).
- ²⁷J. Kirschner, *Surf. Sci.* **138**, 191 (1984).
- ²⁸J. Kirschner, *Polarized Electrons at Surfaces*, Vol. 106 of *Springer Tracts in Modern Physics*, edited by EDITORS (Springer-Verlag, Heidelberg, 1985), p. 30.
- ²⁹J. Kirschner, *Polarized Electrons at Surfaces*, Ref. 28, Chap. 3.
- ³⁰Surface Science Laboratories, Mountain View, CA 94043.
- ³¹J. Kirschner and R. Feder, *Phys. Rev. Lett.* **42**, 1008 (1979).
- ³²B. J. Stocker, *Surf. Sci.* **47**, 501 (1975).
- ³³H.-P. Oepen, Kernforschungsanlage Jülich Report No. Jül-1970, 1985 (unpublished).
- ³⁴R. Feder, A. Rodriguez, U. Baier, and E. Kisker, *Solid State Commun.* **52**, 57, (1984); E. Tamura, R. Feder, and J. Krewer, *ibid.* **55**, 543 (1985); calculations by Wang and Calloway, published in E. Colavita, M. DeCrescenzi, L. Papagno, R. Scarmozzino, L. S. Caputi, R. Rosei, and E. Tosatti, *Phys. Rev. B* **25**, 2490 (1982).
- ³⁵D. R. Penn, *Phys. Rev. B* **35**, 1910 (1987).
- ³⁶J. F. Cooke (private communication).